

RESOLVING THE ELECTRON TEMPERATURE DISCREPANCIES IN H II REGIONS AND PLANETARY NEBULAE: κ -DISTRIBUTED ELECTRONS

DAVID C. NICHOLLS¹, MICHAEL A. DOPITA^{1,2}, AND RALPH S. SUTHERLAND¹

¹ Research School of Astronomy and Astrophysics, Australian National University, Cotter Rd., Weston ACT 2611, Australia; david@mso.anu.edu.au

² Astronomy Department, King Abdulaziz University, P.O. Box 80203, Jeddah, Saudi Arabia

Received 2012 March 6; accepted 2012 April 16; published 2012 June 6

ABSTRACT

The measurement of electron temperatures and metallicities in H II regions and planetary nebulae (PNe) has—for several decades—presented a problem: results obtained using different techniques disagree. What is worse, they disagree consistently. There have been numerous attempts to explain these discrepancies, but none has provided a satisfactory solution to the problem. In this paper, we explore the possibility that electrons in H II regions and PNe depart from a Maxwell–Boltzmann equilibrium energy distribution. We adopt a “ κ -distribution” for the electron energies. Such distributions are widely found in solar system plasmas, where they can be directly measured. This simple assumption is able to explain the temperature and metallicity discrepancies in H II regions and PNe arising from the different measurement techniques. We find that the energy distribution does not need to depart dramatically from an equilibrium distribution. From an examination of data from H II regions and PNe, it appears that $\kappa \gtrsim 10$ is sufficient to encompass nearly all objects. We argue that the kappa-distribution offers an important new insight into the physics of gaseous nebulae, both in the Milky Way and elsewhere, and one that promises significantly more accurate estimates of temperature and metallicity in these regions.

Key words: acceleration of particles – atomic data – atomic processes – H II regions – ISM: abundances – planetary nebulae: general – plasmas

Online-only material: color figures

1. INTRODUCTION

Over 40 years ago, Vasyliunas (1968) measured the electron energy distributions in Earth’s magnetosphere using the OGO1 and OGO3 satellites and found that there was a significant high-energy (suprathermal) excess when compared to an equilibrium Maxwell–Boltzmann (M-B) distribution. The best fit to this high-energy tail was a power law. He introduced the “ κ -distribution”—a generalized Lorentzian distribution—which provided a good description of the electron energy distribution over the full range of energies.

Since then, κ -distributions have been the subject of considerable interest in solar system physics. They have been found by direct measurement of electron energies by satellites and space probes in the outer heliosphere, the magnetospheres of all the gas-giant planets, Mercury and the moons Titan and Io, Earth’s magnetosphere, the plasma sheet and magneto-sheath, and in the Solar Wind (see references in Pierrard & Lazar 2010). Evidence is also emerging from IBEX observations that energetic neutral atoms in the interstellar medium, where it interacts with the heliosheath, exhibit κ -distributions (Livadiotis et al. 2011). More than 5000 papers in many disciplines on the applications of κ -distributions had been published prior to 2011 (Livadiotis & McComas 2011). In solar system plasmas, κ -distributions arise whenever the plasma is being continually pumped by an energy input of a non-thermal or supra-thermal nature, or by energy transport from elsewhere, so that the system cannot relax to a classical M-B distribution.

To date, despite the extensive adoption of κ -distributions in analyzing solar system plasmas—where they are the rule rather than the exception—the possibility that electron energies are distributed in a non-thermal manner in the photoionized plasma of H II regions, planetary nebulae (PNe), or in the photoionized regions around active galaxies, does not appear to have been

considered. Indeed, the assumption that the electrons are in M-B equilibrium dates back over 70 years (see, for example, Hebb & Menzel 1940).

There are good reasons to question the basis on which temperatures and metallicities are measured in H II regions and PNe: for example, there have been consistent discrepancies between direct electron temperature (T_e) estimates and those obtained using recombination lines. None of the earlier attempts to solve the problem are fully satisfactory—for example, the “ t^2 ” temperature fluctuation method (Peimbert 1967)—and some have been completely abandoned (Stasińska 2004).

In this paper, we explore the implications of electron energies following a κ -distribution in these photoionized plasmas. We show that assuming a κ electron energy distribution is a simple and elegant way to resolve many of the difficulties, and should lead to more consistent temperature measurements and metallicity estimates in H II regions and PNe.

The paper is organized as follows. In Section 2, we provide the key definitions and formulae for the κ -distribution. In Section 3, we show that there is a sound basis for H II regions and PNe having κ -distributed electrons. In Section 4, we examine the dependence of collisional excitation rates on excitation energy and the value of κ , and apply this to a detailed study of the particular case of the [O III] $\lambda\lambda(4949 + 5007)/4363$ line ratio, the most important ratio used in the determination of electron temperatures in photoionized plasmas. In Section 5, we summarize the temperature discrepancy problem that has bedeviled temperature and metallicity measurements in gaseous nebulae for decades. In Section 6, we examine the observational data from H II regions and PNe to show how the assumption of a κ -distribution can explain the temperature discrepancies, and how the value of κ can be constrained by requiring that different methods of measuring the electron temperature yield the same answer. Appendix A presents additional evidence for

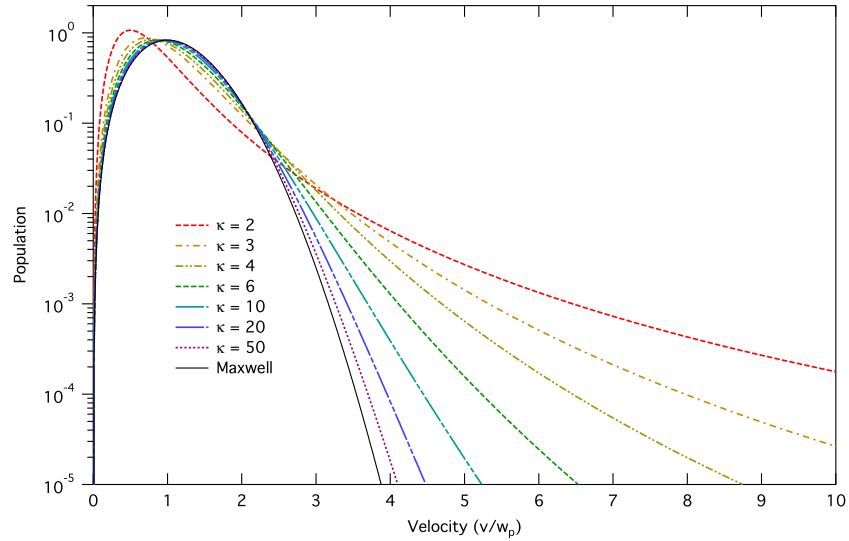


Figure 1. κ velocity distributions (log scale) for κ from 2 to 50, with Maxwell–Boltzmann distribution.

the presence of magnetic fields in H II regions which can give rise to hot-tailed electron energy distributions. In Appendix B, we examine the relationship between the “ t^2 ” method for measuring the effect of temperature fluctuations and the κ -distribution.

2. THE κ -DISTRIBUTION

2.1. Properties and Definitions

Initially, κ -distributions were used as an empirical fit to directly measure electron energies in solar system plasmas, and were criticized as lacking a theoretical basis. More recently, the distribution has been shown to arise from entropic considerations. See, for example, Tsallis et al. (1995), Treumann (1999), Leubner (2002), and the comprehensive analysis by Livadiotis & McComas (2009). They explored the so-called q -nonextensive entropy statistics in which the entropies of adjacent samples of plasma are not simply additive, and have shown that κ energy distributions arise naturally in such plasmas. The requirement for this to occur is that there be long-range interactions between particles, in addition to the short-range Coulombic forces that give rise to M-B equilibration. Although there is ongoing debate over whether the Tsallis statistical mechanics is the best generalization of Boltzmann–Gibbs statistics, it provides a sound physical basis for the overtly successful use of the κ -distribution in plasma physics.

There are a number of slightly differing expressions for the energy distributions that can arise from q -nonextensive entropy, but the forms are generally similar. Here, we adopt the Vasyliunas form of the distribution as representative of the possible variants. This is referred to by Livadiotis & McComas (2009) as a κ -distribution of the “second kind.” The successful use of the κ -distributions to describe physical phenomena in many disciplines, and especially in solar system physics, provides ample justification for exploring their use in H II regions and PNe.

The κ -velocity distribution can be expressed (after Vasyliunas 1968) as

$$n(v)dv = \frac{4N}{\sqrt{\pi}w_0^3} \left(\frac{\Gamma(\kappa+1)}{\kappa^{3/2}\Gamma(\kappa-\frac{1}{2})} \right) \frac{v^2}{(1+v^2/[(\kappa-\frac{3}{2})w_0^2])^{\kappa+1}} dv, \quad (1)$$

where $n(v)$ is the number of electrons with speeds between v and $v+dv$. The velocity w_0 is related to w_{mp} , the most probable speed (i.e., the velocity value at the distribution peak) by

$$w_0 = w_{mp} \left(\frac{\kappa}{(\kappa-\frac{3}{2})} \right)^{1/2} \quad (2)$$

and related to the “physical temperature” of the system, T_U , as defined in Livadiotis & McComas (2009):

$$w_0 = \left(\frac{2k_B T_U}{m_e} \right)^{1/2}, \quad (3)$$

where m_e is the electron mass and k_B is the Boltzmann constant.

κ is a parameter that describes the extent to which the distribution departs from an equilibrium distribution. In the Vasyliunas form, $(3/2) < \kappa \leq \infty$. In the limit as $\kappa \rightarrow \infty$, the velocity distribution reverts to the standard M-B form:

$$n(v)dv = \frac{4N}{\sqrt{\pi}w_0^3} v^2 \exp\left[-\frac{v^2}{w_0^2}\right] dv. \quad (4)$$

The physical temperature, T_U , also referred to as the kinetic temperature, is a generalization of the M-B equilibrium temperature, and is related to the energy density (system kinetic energy), U , which for a monatomic gas is the internal energy of the system:

$$U = \frac{3}{2} k_B T_U. \quad (5)$$

Figure 1 shows a family of κ velocity distributions with an M-B distribution.

Expressed in energy terms, the κ -distribution becomes

$$n(E)dE = \frac{2N}{\sqrt{\pi}} \left(\frac{\Gamma(\kappa+1)}{(\kappa-\frac{3}{2})^{3/2}\Gamma(\kappa-\frac{1}{2})} \right) \times \frac{\sqrt{E}}{(k_B T_U)^{3/2} (1+E/[(\kappa-\frac{3}{2})k_B T_U])^{\kappa+1}} dE. \quad (6)$$

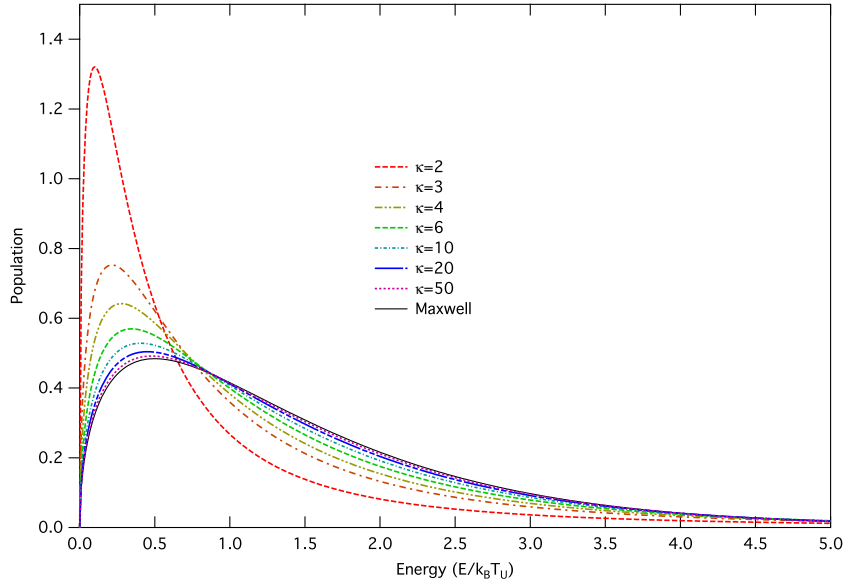


Figure 2. κ energy distributions (linear scale) for κ from 2 to 50, with Maxwell–Boltzmann distribution.

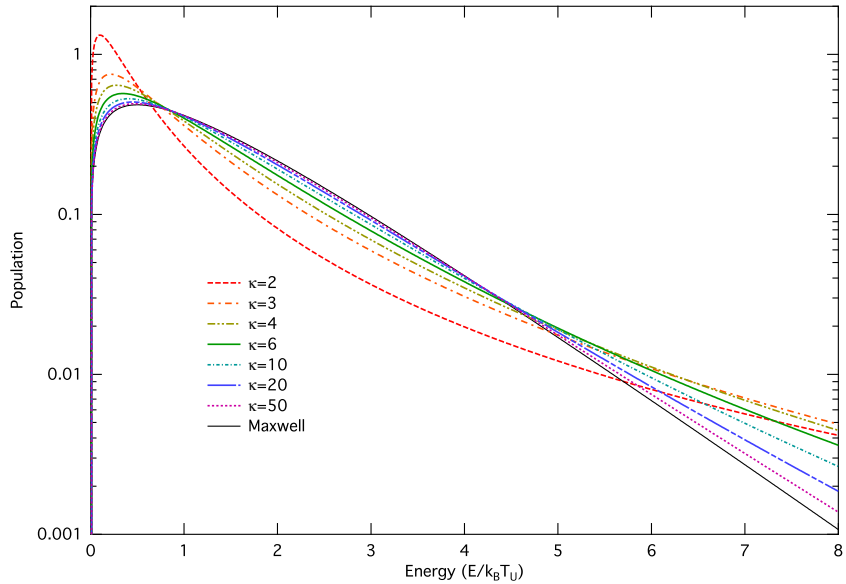


Figure 3. κ energy distributions (log scale) for κ from 2 to 50, with Maxwell–Boltzmann distribution.

Again, the κ energy distribution tends in the limit as $\kappa \rightarrow \infty$ to the M-B:

$$n(E)dE = \frac{2N}{\sqrt{\pi}} \frac{\sqrt{E} \exp[-E/k_B T]}{(k_B T)^{3/2}} dE. \quad (7)$$

A family of normalized κ energy distributions is shown in Figure 2, together with an M-B equilibrium distribution. Note that the peak of the M-B energy distribution occurs at $E = (1/2)k_B T_U$, whereas κ -distributions with the same internal energy peak at $E = (1/2)k_B T_U (2\kappa - 3)/(2\kappa + 1)$.

The same distributions are shown in Figure 3 but plotted on a log scale. The high-energy power-law tail of the κ -distributions is clearly shown.

Figures 1–3 illustrate the key characteristics of the κ -distribution: the peak of the distribution moves to lower energies; at intermediate energies there is a population deficit relative to the M-B distribution; and at higher energies the “hot tail” again provides a population excess over the M-B.

The κ -distribution behaves as an M-B distribution at a lower temperature, but with a significant high-energy excess.

This can be seen in Figure 4, where an M-B distribution is peak-fitted to a $\kappa = 2$ distribution. The peak-fitted “core” M-B distribution is in fact at a lower physical temperature than the κ -distribution to which it is fitted. The low-energy “core” occurs because the equilibration timescale is a strong function of energy ($\propto \exp E^{3/2}$), allowing the low-energy electrons to approach an equilibrium distribution. The relationship between the physical temperature of the κ -distribution, T_U , and the equilibrium temperature of the “core” M-B, T_{core} , as implied by Equation (3), is

$$T_{\text{core}} = T_U \left(\frac{\kappa - \frac{3}{2}}{\kappa} \right). \quad (8)$$

For physical processes that involve low-energy electrons such as recombination line excitation, reactions “see” the cool

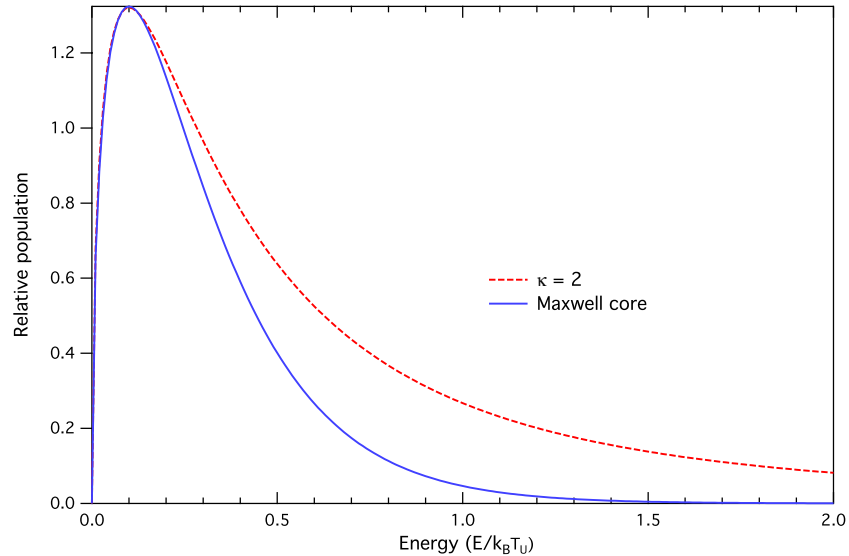


Figure 4. $\kappa = 2$ energy distribution with peak-fitted Maxwell–Boltzmann distribution core.

M-B core distribution. In other words, any physical property sensitive to the region of the electron energy distribution around or below the distribution peak will interact with an effective M-B electron energy distribution at a lower temperature than the M-B distribution with the same total internal energy as the κ -distribution.

Conversely, in processes that depend on the high energy end of the distribution, such as collisional line excitation, the κ -distribution behaves like an M-B distribution at a higher temperature than one with the same total internal energy. In other words, physical properties sensitive to energies above the peak will behave as if they were interacting with a hotter distribution. The κ -distribution thus exhibits a “split personality,” depending on the physical process involved. We show below that this behavior resolves many of the discrepancies between different nebular temperature measurement techniques.

3. WHAT MIGHT GIVE RISE TO κ -DISTRIBUTIONS IN H II REGIONS?

Given the plausibility of κ -distributions in H II regions, can we find mechanisms capable of maintaining the hot tails? The answer is, clearly, yes. A high-energy tail in the energy distribution will occur whenever the population of energetic electrons is being pumped in a timescale as short, or of the same order, as the energy redistribution timescale of the electron population. Such effects may be long range in nature, such as magnetic reconnection followed by the migration of high-energy electrons along field lines, and by the development of inertial Alfvén waves. We explore additional evidence for the existence of magnetic fields in galactic H II regions in Appendix A.

Pumping of high-energy tails can also be more local in character, such as local shocks (driven either by the collision of bulk flows or by supersonic turbulence), or, most simply, by the injection of high-energy electrons through the photoionization process itself. Normal photoionization produces supra-thermal electrons on a timescale similar to the recombination timescale.

Energetic electrons can also be generated by the photoionization of dust (Dopita & Sutherland 2000). Alternatively, X-ray ionization can produce highly energetic (\sim keV) inner-shell (Auger process) electrons (e.g., Shull & Van Steenberg 1985; Aldrovandi & Gruenwald 1985; Petrini & Da Silva 1997

and references therein). Processes based on photoionization should become more effective where the source of the ionizing photons has a “hard” photon spectrum. Thus, the likelihood of the ionized plasma having a κ electron energy distribution would be high in the case of either photoionization by an active galactic nucleus (AGN), or the case of PNe, in which the effective temperature of the exciting star could range up to \sim 250,000 K.

Thus, we have no shortage of possible energy injection mechanisms. The main consideration is whether feeding the energetic population can occur on a timescale which is short compared with the collisional redistribution timescale, τ . Because this timescale increases very rapidly with energy, $\tau \propto \exp(E^{3/2})$, we would expect there to be a threshold energy above which any non-thermal electrons have a long residence timescale. These can then feed continually down toward lower energies, maintaining a κ electron energy distribution. It seems more likely therefore that *all* photoionized plasmas will show departures from an M-B distribution to some degree. The key question is, is this departure important, and does it produce observable effects in the plasma diagnostics on which we have relied upon hitherto? Again, yes, as we show in Section 4 below.

3.1. Are κ -distributions Stable in Their Own Right?

In addition to the energy injection mechanisms capable of maintaining the excitation of suprathermal distributions, several authors (Livadiotis & McComas 2011 and references therein; Shizgal 2007; Treumann 2001) have investigated the possibility that the κ -distribution may remain stable against thermalization longer than conventional thermalization considerations would suggest (e.g., Spitzer 1962). In particular, distributions with $2.5 \gtrsim \kappa > 1.5$ appear to have the capacity, through increasing entropy, of moving to values of lower κ (Livadiotis & McComas 2011) i.e., away from (M-B) equilibrium. While the physical application of this aspect of κ -distributions remains to be explored fully, it suggests that where q -nonextensive entropy conditions operate, the suprathermal energy distributions produced exist in “stationary states” where the behavior is, at least in the short term, time-invariant (Livadiotis & McComas 2010). These states may have longer lifetimes than expected classically. This is fully consistent with the numerous observations that in solar system plasmas, κ electron and proton energy distributions

are the norm. It seems reasonable to expect that such conditions will also be present in H II regions and PNe.

4. THE EFFECT OF κ -DISTRIBUTIONS ON COLLISIONAL EXCITATION IN H II REGIONS

4.1. Collisional Excitation Rates

Consider the collisional excitation of an atomic species from energy level 1 to energy level 2. The rate of collisional population of the upper energy level per unit volume is given in terms of the collision cross-section, $\sigma_{12}(E)$, by

$$R_{12} = n_e N_1 \int_{E_{12}}^{\infty} \sigma_{12}(E) \sqrt{E} f(E) dE. \quad (9)$$

We separate out the strong energy dependence of the collision cross-section $\sigma_{12}(E)$, by expressing it in terms of the collision strength, Ω_{12} and the energy, E :

$$\sigma_{12}(E) = \left(\frac{h^2}{8\pi m_e E} \right) \frac{\Omega_{12}}{g_1}, \quad (10)$$

where h is the Planck Constant, m_e is the electron mass, and g_1 is the statistical weight of the lower energy state.

The collisional population rate now becomes

$$R_{12} = n_e N_1 \frac{h^2}{8\pi m_e g_1} \int_{E_{12}}^{\infty} \frac{\Omega_{12}}{\sqrt{E}} f(E) dE, \quad (11)$$

where the appropriate form of the distribution is substituted, giving the well-known collisional population rate formula for an M-B distribution:

$$R_{12}(\text{M-B}) = n_e N_1 \frac{h^2}{4\pi^{3/2} m_e g_1} (k_B T_U)^{-3/2} \times \int_{E_{12}}^{\infty} \Omega_{12} \exp\left[-\frac{E}{k_B T_U}\right] dE. \quad (12)$$

For a κ -distribution, the corresponding rate is

$$R_{12}(\kappa) = n_e N_1 \frac{h^2}{4\pi^{3/2} m_e g_1} \frac{\Gamma(\kappa + 1)}{(\kappa - \frac{3}{2})^{3/2} \Gamma(\kappa - \frac{1}{2})} (k_B T_U)^{-3/2} \times \int_{E_{12}}^{\infty} \frac{\Omega_{12}}{(1 + E/[(\kappa - \frac{3}{2})k_B T_U])^{\kappa+1}} dE. \quad (13)$$

Adopting the approximation that Ω_{12} is independent of energy, the integral parts of the above equations (after taking a $k_B T_U$ factor outside the integrals) reduce to

$$\exp\left[-\frac{E_{12}}{k_B T_U}\right] \quad (14)$$

and

$$\left(1 - \frac{3}{2\kappa}\right) \left(1 + \frac{E_{12}}{(\kappa - \frac{3}{2})k_B T_U}\right)^{-\kappa}, \quad (15)$$

respectively. Note that in the limit as $\kappa \rightarrow \infty$, Equation (15) transforms into Equation (14), as it should.

It is useful to compare the relative rates of population to an upper state for M-B and κ -distributions. Taking Equations (12)

and (13) and assuming constant Ω_{12} , we can derive an analytical equation that expresses the ratio of the population rates:

$$\frac{R_{12}(\kappa)}{R_{12}(\text{M-B})} = \frac{\Gamma(\kappa + 1)}{(\kappa - \frac{3}{2})^{3/2} \Gamma(\kappa - \frac{1}{2})} \left(1 - \frac{3}{2\kappa}\right) \times \exp\left[\frac{E_{12}}{k_B T_U}\right] \left(1 + \frac{E_{12}}{(\kappa - \frac{3}{2})k_B T_U}\right)^{-\kappa}. \quad (16)$$

Figure 5 shows the effect of Equation (16) in the enhancement of the collisional excitation rate for $\kappa: 2 \rightarrow 100$ compared to the M-B rate for an electron distribution having the same internal energy. Very similar curves were obtained by Owoki & Scudder (1983) in the context of collisional ionization rates in the solar corona. Data for Figure 5 for an extended energy ratio range are given in Table 1.

The implication is that collisionally excited UV lines—with higher excitation energies—should show strong enhancements compared to standard theory, while lines in the optical and IR would be relatively little changed, unless the region has a low kinetic temperature. Collisionally excited lines of non-ionized species such as [O I] $\lambda\lambda 6300, 63$ or [N I] $\lambda\lambda 5198, 5200$ will be differently affected, since the collision strength has a strong energy dependence, increasing above threshold. For these ions, the degree of enhancement in the collisional excitation rate compared with the M-B case will be much larger than shown in Figure 6. This could explain a long-standing problem in H II region models, which tend to systematically underestimate the strength of these lines, compared to observations. New data on the collision strengths of O I and N I, in the context of the κ -distribution, have implications for using the lines of these neutral species as low-temperature diagnostics in partially ionized regions. We will explore this in a future paper.

4.2. Effect of κ on [O III] Electron Temperatures

The direct method of estimating electron temperature in H II regions relies on measuring the flux ratios of different excited states from the same atomic species. Most often used are collisional excitation to the 1D_2 and 1S_0 states of [O III], which give rise to the forbidden nebular lines at 5007 Å and 4959 Å, and the “auroral” line at 4363 Å. Lines of [O II], [N II], [S II], [Ne III], [Ar III], and [S III] are also used, when the relevant lines can be observed. The threshold excitation energies for the upper states in these species are different, so the degree of enhancement in a κ -distribution of electrons will differ from one ion to the next. This fact provides a possible resolution of the discrepancies encountered when measuring temperatures using these different atomic species.

As a specific and important example, we consider here the excitation of the O III ion. For reference, the configuration of the lower states which give rise to the forbidden lines used in temperature determinations is illustrated in Figure 6. The threshold excitation temperatures of the excited states are 29,130 K (1D_2) and 62,094 K (1S_0). For a κ -distribution at temperature $T_U = 10,000$ K from Figure 5, the excitation rate to the lower state will be little changed, while the collision excitation rate to the upper state will be strongly enhanced, leading to an overestimate of the true electron temperature computed by formulae such as given by Osterbrock & Ferland (2005). We now proceed to quantify this remark.

For an equilibrium electron energy distribution, the relative population rates can be calculated using Equation (11) for the upper and lower excited states. If one assumes for simplicity

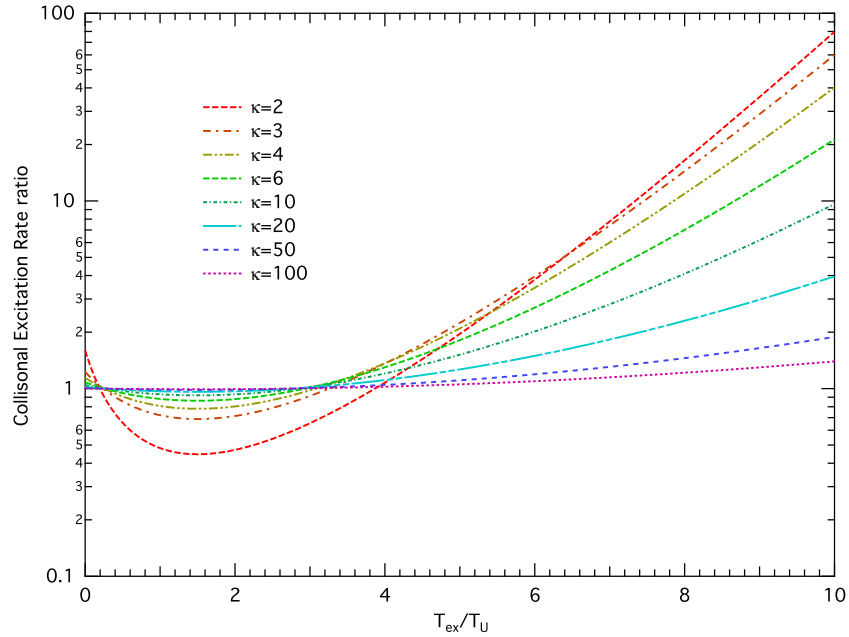


Figure 5. Collisional excitation enhancement ratio over a Maxwell–Boltzmann distribution for different κ -distributions plotted as a function of the excitation threshold energy (expressed as an equivalent temperature) over the kinetic temperature T_U (Equation (16)). For the κ -distributions, very large enhancements in the collisional excitation rate are possible for high values of T_{ex}/T_U . (extended data in Table 1.)



Figure 6. Lower energy levels and forbidden transitions for the O III ion.

that the Ω values are energy-independent, then the ratio of the two population rates in the M-B case is simply

$$\frac{R_{13}}{R_{12}} = \frac{\Omega_{13}}{\Omega_{12}} \exp\left[-\frac{E_{23}}{k_B T_U}\right]. \quad (17)$$

In a more accurate analysis, the collision strength Ω is integrated over the energy range E_{12} to ∞ as per Equation (11), to give the effective (temperature averaged) collision strength, Υ .

Allowing for other transitions from the 1S_0 state via the branching ratio and correcting for the energies of the two lower state transition photons, the ratio of the fluxes of the ($\lambda 5007 + \lambda 4959$) to $\lambda 4363$ give a direct measure of the population rates to the two excited states, and therefore of the electron temperature of the energy distribution. Following Osterbrock & Ferland (2005), we can derive a simple equation for the electron temperature, T_e , in terms of the line fluxes, for low density plasmas:

$$\frac{j_{5007} + j_{4959}}{j_{4363}} = 7.90 \exp\left[\frac{32900}{T_e}\right]. \quad (18)$$

This formula is, of course, an approximation, as it assumes the values Ω_{12} and Ω_{13} (and therefore of Υ_{12} and Υ_{13}) do not depend

on temperature. A more accurate iterative formula was given by Izotov et al. (2006). Values of the effective collision strength Υ , assuming constant Ω , differ slightly from those computed numerically, taking into account the detailed collisional cross-section resonances. To identify what effect this would have on determining the electron temperature, we compared electron temperatures derived using constant Ω , the Izotov iterated formula, and the values computed using the detailed collision strengths from Lennon & Burke (1994) and Aggarwal (1993).

Figure 7 shows the relationship between the flux ratio and the electron temperature, using the Osterbrock equation, the Izotov iteration, and computed numerically from the Lennon & Burke (1994) and Aggarwal (1993) Ω data. (The values in most common use for Υ_{12} are those published by Lennon & Burke 1994, available online via TIPbase (Hummer et al. 1993); or the data from Aggarwal & Keenan 1999, but the latter are only available in abbreviated tabular form.)

For M-B energy distributions, the use of a constant Ω gives a slightly higher T_e than is obtained using the Lennon & Burke (1994) data, and higher still compared to the data from Aggarwal (1993). At an equilibrium temperature of 20,000 K, the difference between the Izotov value and the L&B data is 130 K and for the Aggarwal data, 285 K.

These differences are of minor import. An altogether different result occurs when we use a κ -distribution instead of the M-B to calculate the line ratio versus T_U graph. The results are shown in Figure 8. For $\kappa = 100, 50, 20$, and 10 the kinetic temperature differences from the M-B equilibrium value at $T_U = 20,000$ K are 180 K, 385 K, 980 K, and 2100 K. Data for the extended temperature range 5000–20,000 K are given in Table 2. The data are calculated using the detailed collision strengths (from Lennon & Burke 1994), but assuming constant Ω s makes only a small difference for $\kappa > 6$.

As can be seen in Figures 2 and 3, these values of κ are visually relatively minor deviations from the M-B distribution, but they have a considerable effect. This implies that even κ -distributions which diverge slightly from equilibrium can have

Table 1
Collisional Excitation Rate Ratios (See Figure 5)

T_{ex}/T_U	$\kappa = 2$	$\kappa = 3$	$\kappa = 4$	$\kappa = 6$	$\kappa = 10$	$\kappa = 20$	$\kappa = 50$	$\kappa = 100$
0.0	1.596E+00	1.228E+00	1.142E+00	1.081E+00	1.043E+00	1.020E+00	1.008E+00	1.004E+00
0.1	1.225E+00	1.119E+00	1.079E+00	1.047E+00	1.026E+00	1.012E+00	1.005E+00	1.002E+00
0.2	9.944E-01	1.031E+00	1.025E+00	1.017E+00	1.010E+00	1.005E+00	1.002E+00	1.001E+00
0.3	8.414E-01	9.596E-01	9.795E-01	9.905E-01	9.956E-01	9.982E-01	9.994E-01	9.997E-01
0.4	7.348E-01	9.017E-01	9.408E-01	9.672E-01	9.828E-01	9.921E-01	9.970E-01	9.985E-01
0.5	6.577E-01	8.544E-01	9.079E-01	9.469E-01	9.713E-01	9.866E-01	9.949E-01	9.975E-01
0.6	6.008E-01	8.157E-01	8.800E-01	9.293E-01	9.612E-01	9.817E-01	9.929E-01	9.965E-01
0.7	5.579E-01	7.841E-01	8.566E-01	9.141E-01	9.523E-01	9.774E-01	9.912E-01	9.957E-01
0.8	5.254E-01	7.584E-01	8.370E-01	9.011E-01	9.446E-01	9.736E-01	9.897E-01	9.949E-01
0.9	5.006E-01	7.377E-01	8.209E-01	8.902E-01	9.380E-01	9.703E-01	9.884E-01	9.943E-01
1.0	4.820E-01	7.213E-01	8.080E-01	8.813E-01	9.326E-01	9.676E-01	9.873E-01	9.937E-01
1.1	4.682E-01	7.086E-01	7.978E-01	8.742E-01	9.282E-01	9.654E-01	9.864E-01	9.933E-01
1.2	4.583E-01	6.993E-01	7.902E-01	8.688E-01	9.248E-01	9.636E-01	9.857E-01	9.929E-01
1.3	4.518E-01	6.930E-01	7.849E-01	8.650E-01	9.225E-01	9.624E-01	9.852E-01	9.927E-01
1.4	4.481E-01	6.894E-01	7.818E-01	8.628E-01	9.211E-01	9.617E-01	9.849E-01	9.925E-01
1.5	4.470E-01	6.882E-01	7.808E-01	8.620E-01	9.206E-01	9.614E-01	9.848E-01	9.925E-01
1.6	4.481E-01	6.893E-01	7.818E-01	8.628E-01	9.211E-01	9.617E-01	9.849E-01	9.925E-01
1.7	4.512E-01	6.926E-01	7.846E-01	8.649E-01	9.224E-01	9.624E-01	9.852E-01	9.927E-01
1.8	4.562E-01	6.979E-01	7.893E-01	8.683E-01	9.247E-01	9.636E-01	9.857E-01	9.929E-01
1.9	4.631E-01	7.053E-01	7.956E-01	8.731E-01	9.278E-01	9.652E-01	9.864E-01	9.933E-01
2.0	4.716E-01	7.145E-01	8.037E-01	8.792E-01	9.318E-01	9.674E-01	9.873E-01	9.937E-01
2.1	4.819E-01	7.257E-01	8.135E-01	8.866E-01	9.367E-01	9.700E-01	9.884E-01	9.942E-01
2.2	4.939E-01	7.387E-01	8.249E-01	8.953E-01	9.424E-01	9.730E-01	9.896E-01	9.949E-01
2.3	5.075E-01	7.536E-01	8.381E-01	9.054E-01	9.490E-01	9.765E-01	9.911E-01	9.956E-01
2.4	5.229E-01	7.704E-01	8.529E-01	9.167E-01	9.565E-01	9.805E-01	9.927E-01	9.965E-01
2.5	5.400E-01	7.892E-01	8.694E-01	9.293E-01	9.648E-01	9.850E-01	9.946E-01	9.974E-01
2.6	5.589E-01	8.099E-01	8.877E-01	9.432E-01	9.740E-01	9.899E-01	9.966E-01	9.984E-01
2.7	5.797E-01	8.327E-01	9.077E-01	9.585E-01	9.841E-01	9.953E-01	9.989E-01	9.996E-01
2.8	6.024E-01	8.575E-01	9.296E-01	9.752E-01	9.951E-01	1.001E+00	1.001E+00	1.001E+00
2.9	6.272E-01	8.845E-01	9.533E-01	9.932E-01	1.007E+00	1.008E+00	1.004E+00	1.002E+00
3.0	6.541E-01	9.138E-01	9.790E-01	1.013E+00	1.020E+00	1.014E+00	1.007E+00	1.004E+00
3.1	6.833E-01	9.455E-01	1.007E+00	1.034E+00	1.034E+00	1.022E+00	1.010E+00	1.005E+00
3.2	7.149E-01	9.796E-01	1.037E+00	1.056E+00	1.048E+00	1.030E+00	1.013E+00	1.007E+00
3.3	7.491E-01	1.016E+00	1.069E+00	1.080E+00	1.064E+00	1.038E+00	1.017E+00	1.009E+00
3.4	7.859E-01	1.056E+00	1.103E+00	1.106E+00	1.081E+00	1.047E+00	1.020E+00	1.010E+00
3.5	8.257E-01	1.098E+00	1.140E+00	1.134E+00	1.099E+00	1.056E+00	1.024E+00	1.012E+00
3.6	8.686E-01	1.144E+00	1.179E+00	1.163E+00	1.118E+00	1.066E+00	1.028E+00	1.014E+00
3.7	9.147E-01	1.193E+00	1.221E+00	1.194E+00	1.137E+00	1.076E+00	1.032E+00	1.016E+00
3.8	9.645E-01	1.245E+00	1.266E+00	1.227E+00	1.159E+00	1.087E+00	1.037E+00	1.019E+00
3.9	1.018E+00	1.301E+00	1.313E+00	1.262E+00	1.181E+00	1.099E+00	1.041E+00	1.021E+00
4.0	1.076E+00	1.361E+00	1.364E+00	1.299E+00	1.204E+00	1.111E+00	1.046E+00	1.023E+00
4.1	1.138E+00	1.425E+00	1.418E+00	1.339E+00	1.229E+00	1.123E+00	1.051E+00	1.026E+00
4.2	1.204E+00	1.493E+00	1.476E+00	1.380E+00	1.255E+00	1.137E+00	1.057E+00	1.029E+00
4.3	1.276E+00	1.566E+00	1.537E+00	1.424E+00	1.282E+00	1.150E+00	1.062E+00	1.031E+00
4.4	1.353E+00	1.644E+00	1.603E+00	1.471E+00	1.311E+00	1.165E+00	1.068E+00	1.034E+00
4.5	1.437E+00	1.728E+00	1.672E+00	1.520E+00	1.341E+00	1.180E+00	1.074E+00	1.037E+00
4.6	1.526E+00	1.817E+00	1.746E+00	1.572E+00	1.373E+00	1.196E+00	1.080E+00	1.040E+00
4.7	1.622E+00	1.913E+00	1.825E+00	1.627E+00	1.406E+00	1.212E+00	1.087E+00	1.044E+00
4.8	1.726E+00	2.015E+00	1.909E+00	1.685E+00	1.441E+00	1.229E+00	1.093E+00	1.047E+00
4.9	1.837E+00	2.124E+00	1.998E+00	1.747E+00	1.478E+00	1.247E+00	1.100E+00	1.050E+00
5.0	1.957E+00	2.241E+00	2.092E+00	1.812E+00	1.516E+00	1.265E+00	1.107E+00	1.054E+00
5.1	2.087E+00	2.365E+00	2.193E+00	1.881E+00	1.557E+00	1.285E+00	1.115E+00	1.057E+00
5.2	2.226E+00	2.499E+00	2.300E+00	1.953E+00	1.599E+00	1.305E+00	1.122E+00	1.061E+00
5.3	2.376E+00	2.642E+00	2.414E+00	2.030E+00	1.643E+00	1.325E+00	1.130E+00	1.065E+00
5.4	2.537E+00	2.794E+00	2.535E+00	2.110E+00	1.689E+00	1.347E+00	1.138E+00	1.069E+00
5.5	2.712E+00	2.958E+00	2.665E+00	2.196E+00	1.738E+00	1.369E+00	1.146E+00	1.073E+00
5.6	2.899E+00	3.133E+00	2.802E+00	2.286E+00	1.789E+00	1.393E+00	1.155E+00	1.077E+00
5.7	3.102E+00	3.320E+00	2.948E+00	2.382E+00	1.842E+00	1.417E+00	1.164E+00	1.081E+00
5.8	3.320E+00	3.520E+00	3.104E+00	2.482E+00	1.898E+00	1.442E+00	1.173E+00	1.086E+00
5.9	3.555E+00	3.735E+00	3.270E+00	2.589E+00	1.956E+00	1.468E+00	1.183E+00	1.090E+00
6.0	3.809E+00	3.965E+00	3.447E+00	2.702E+00	2.017E+00	1.495E+00	1.192E+00	1.095E+00
6.1	4.083E+00	4.211E+00	3.636E+00	2.821E+00	2.081E+00	1.523E+00	1.202E+00	1.100E+00
6.2	4.379E+00	4.475E+00	3.836E+00	2.947E+00	2.148E+00	1.552E+00	1.213E+00	1.105E+00
6.3	4.698E+00	4.758E+00	4.050E+00	3.080E+00	2.219E+00	1.582E+00	1.223E+00	1.110E+00
6.4	5.043E+00	5.061E+00	4.279E+00	3.221E+00	2.292E+00	1.613E+00	1.234E+00	1.115E+00

Table 1
(Continued)

T_{ex}/T_U	$\kappa = 2$	$\kappa = 3$	$\kappa = 4$	$\kappa = 6$	$\kappa = 10$	$\kappa = 20$	$\kappa = 50$	$\kappa = 100$
6.5	5.415E+00	5.386E+00	4.522E+00	3.369E+00	2.369E+00	1.645E+00	1.245E+00	1.120E+00
6.6	5.818E+00	5.735E+00	4.781E+00	3.527E+00	2.450E+00	1.679E+00	1.257E+00	1.126E+00
6.7	6.252E+00	6.109E+00	5.058E+00	3.694E+00	2.535E+00	1.713E+00	1.268E+00	1.131E+00
6.8	6.722E+00	6.510E+00	5.354E+00	3.870E+00	2.624E+00	1.749E+00	1.281E+00	1.137E+00
6.9	7.229E+00	6.941E+00	5.669E+00	4.057E+00	2.717E+00	1.787E+00	1.293E+00	1.143E+00
7.0	7.778E+00	7.403E+00	6.005E+00	4.255E+00	2.814E+00	1.825E+00	1.306E+00	1.148E+00
7.1	8.371E+00	7.900E+00	6.365E+00	4.464E+00	2.917E+00	1.865E+00	1.319E+00	1.154E+00
7.2	9.013E+00	8.433E+00	6.748E+00	4.686E+00	3.024E+00	1.907E+00	1.332E+00	1.161E+00
7.3	9.707E+00	9.006E+00	7.158E+00	4.921E+00	3.136E+00	1.950E+00	1.346E+00	1.167E+00
7.4	1.046E+01	9.621E+00	7.596E+00	5.170E+00	3.254E+00	1.995E+00	1.360E+00	1.173E+00
7.5	1.127E+01	1.028E+01	8.064E+00	5.434E+00	3.378E+00	2.041E+00	1.375E+00	1.180E+00
7.6	1.215E+01	1.099E+01	8.565E+00	5.714E+00	3.508E+00	2.089E+00	1.390E+00	1.187E+00
7.7	1.310E+01	1.176E+01	9.100E+00	6.010E+00	3.644E+00	2.139E+00	1.405E+00	1.194E+00
7.8	1.413E+01	1.258E+01	9.672E+00	6.325E+00	3.787E+00	2.190E+00	1.421E+00	1.201E+00
7.9	1.525E+01	1.346E+01	1.028E+01	6.659E+00	3.937E+00	2.244E+00	1.437E+00	1.208E+00
8.0	1.646E+01	1.441E+01	1.094E+01	7.013E+00	4.094E+00	2.299E+00	1.453E+00	1.215E+00
8.1	1.777E+01	1.544E+01	1.164E+01	7.389E+00	4.259E+00	2.356E+00	1.470E+00	1.223E+00
8.2	1.919E+01	1.654E+01	1.239E+01	7.787E+00	4.433E+00	2.416E+00	1.488E+00	1.230E+00
8.3	2.073E+01	1.773E+01	1.319E+01	8.211E+00	4.615E+00	2.478E+00	1.505E+00	1.238E+00
8.4	2.240E+01	1.900E+01	1.405E+01	8.660E+00	4.807E+00	2.542E+00	1.524E+00	1.246E+00
8.5	2.421E+01	2.038E+01	1.497E+01	9.138E+00	5.008E+00	2.608E+00	1.542E+00	1.254E+00
8.6	2.617E+01	2.186E+01	1.596E+01	9.645E+00	5.219E+00	2.677E+00	1.562E+00	1.263E+00
8.7	2.829E+01	2.345E+01	1.702E+01	1.018E+01	5.441E+00	2.748E+00	1.581E+00	1.271E+00
8.8	3.060E+01	2.517E+01	1.815E+01	1.076E+01	5.675E+00	2.822E+00	1.601E+00	1.280E+00
8.9	3.310E+01	2.702E+01	1.936E+01	1.137E+01	5.921E+00	2.899E+00	1.622E+00	1.288E+00
9.0	3.582E+01	2.902E+01	2.066E+01	1.201E+01	6.179E+00	2.979E+00	1.643E+00	1.297E+00
9.1	3.877E+01	3.117E+01	2.206E+01	1.270E+01	6.450E+00	3.062E+00	1.665E+00	1.307E+00
9.2	4.196E+01	3.350E+01	2.356E+01	1.343E+01	6.736E+00	3.148E+00	1.687E+00	1.316E+00
9.3	4.544E+01	3.600E+01	2.516E+01	1.421E+01	7.037E+00	3.237E+00	1.710E+00	1.325E+00
9.4	4.920E+01	3.870E+01	2.689E+01	1.504E+01	7.353E+00	3.329E+00	1.733E+00	1.335E+00
9.5	5.330E+01	4.161E+01	2.874E+01	1.592E+01	7.686E+00	3.426E+00	1.757E+00	1.345E+00
9.6	5.774E+01	4.476E+01	3.072E+01	1.686E+01	8.037E+00	3.525E+00	1.782E+00	1.355E+00
9.7	6.257E+01	4.815E+01	3.285E+01	1.786E+01	8.406E+00	3.629E+00	1.807E+00	1.365E+00
9.8	6.781E+01	5.182E+01	3.514E+01	1.893E+01	8.794E+00	3.736E+00	1.833E+00	1.376E+00
9.9	7.351E+01	5.577E+01	3.760E+01	2.006E+01	9.204E+00	3.848E+00	1.859E+00	1.386E+00
10.0	7.970E+01	6.004E+01	4.024E+01	2.127E+01	9.635E+00	3.964E+00	1.886E+00	1.397E+00
10.1	8.643E+01	6.466E+01	4.308E+01	2.256E+01	1.009E+01	4.085E+00	1.914E+00	1.408E+00
10.2	9.374E+01	6.964E+01	4.613E+01	2.393E+01	1.057E+01	4.210E+00	1.942E+00	1.420E+00
10.3	1.017E+02	7.503E+01	4.940E+01	2.539E+01	1.107E+01	4.340E+00	1.972E+00	1.431E+00
10.4	1.103E+02	8.084E+01	5.293E+01	2.695E+01	1.161E+01	4.475E+00	2.001E+00	1.443E+00
10.5	1.197E+02	8.713E+01	5.671E+01	2.861E+01	1.217E+01	4.616E+00	2.032E+00	1.455E+00
10.6	1.300E+02	9.393E+01	6.079E+01	3.038E+01	1.276E+01	4.762E+00	2.063E+00	1.467E+00
10.7	1.411E+02	1.013E+02	6.517E+01	3.228E+01	1.338E+01	4.913E+00	2.096E+00	1.479E+00
10.8	1.532E+02	1.092E+02	6.988E+01	3.429E+01	1.404E+01	5.071E+00	2.129E+00	1.492E+00
10.9	1.663E+02	1.178E+02	7.495E+01	3.645E+01	1.474E+01	5.235E+00	2.162E+00	1.504E+00
11.0	1.806E+02	1.271E+02	8.040E+01	3.875E+01	1.547E+01	5.406E+00	2.197E+00	1.517E+00
11.1	1.962E+02	1.371E+02	8.627E+01	4.120E+01	1.625E+01	5.584E+00	2.232E+00	1.531E+00
11.2	2.131E+02	1.480E+02	9.259E+01	4.382E+01	1.706E+01	5.768E+00	2.269E+00	1.544E+00
11.3	2.316E+02	1.598E+02	9.940E+01	4.662E+01	1.793E+01	5.961E+00	2.306E+00	1.558E+00
11.4	2.516E+02	1.725E+02	1.067E+02	4.961E+01	1.884E+01	6.161E+00	2.344E+00	1.572E+00
11.5	2.735E+02	1.863E+02	1.146E+02	5.280E+01	1.980E+01	6.369E+00	2.384E+00	1.586E+00
11.6	2.973E+02	2.012E+02	1.231E+02	5.622E+01	2.082E+01	6.585E+00	2.424E+00	1.601E+00
11.7	3.232E+02	2.173E+02	1.323E+02	5.986E+01	2.190E+01	6.811E+00	2.465E+00	1.616E+00
11.8	3.514E+02	2.348E+02	1.421E+02	6.376E+01	2.303E+01	7.045E+00	2.507E+00	1.631E+00
11.9	3.821E+02	2.538E+02	1.528E+02	6.793E+01	2.423E+01	7.290E+00	2.551E+00	1.646E+00
12.0	4.156E+02	2.743E+02	1.642E+02	7.238E+01	2.551E+01	7.544E+00	2.595E+00	1.662E+00
12.1	4.520E+02	2.965E+02	1.766E+02	7.715E+01	2.685E+01	7.809E+00	2.641E+00	1.678E+00
12.2	4.917E+02	3.205E+02	1.899E+02	8.224E+01	2.827E+01	8.086E+00	2.688E+00	1.694E+00
12.3	5.349E+02	3.466E+02	2.042E+02	8.769E+01	2.977E+01	8.373E+00	2.736E+00	1.711E+00
12.4	5.821E+02	3.748E+02	2.197E+02	9.352E+01	3.136E+01	8.673E+00	2.785E+00	1.727E+00
12.5	6.334E+02	4.054E+02	2.364E+02	9.977E+01	3.305E+01	8.985E+00	2.835E+00	1.744E+00
12.6	6.894E+02	4.386E+02	2.544E+02	1.064E+02	3.483E+01	9.311E+00	2.887E+00	1.762E+00
12.7	7.504E+02	4.746E+02	2.739E+02	1.136E+02	3.671E+01	9.650E+00	2.940E+00	1.780E+00
12.8	8.169E+02	5.136E+02	2.948E+02	1.213E+02	3.871E+01	1.000E+01	2.995E+00	1.798E+00
12.9	8.894E+02	5.558E+02	3.175E+02	1.294E+02	4.082E+01	1.037E+01	3.051E+00	1.816E+00

Table 1
(Continued)

T_{ex}/T_U	$\kappa = 2$	$\kappa = 3$	$\kappa = 4$	$\kappa = 6$	$\kappa = 10$	$\kappa = 20$	$\kappa = 50$	$\kappa = 100$
13.0	9.684E+02	6.017E+02	3.419E+02	1.382E+02	4.306E+01	1.076E+01	3.108E+00	1.835E+00
13.1	1.055E+03	6.514E+02	3.682E+02	1.476E+02	4.543E+01	1.116E+01	3.167E+00	1.854E+00
13.2	1.149E+03	7.053E+02	3.967E+02	1.577E+02	4.794E+01	1.158E+01	3.227E+00	1.873E+00
13.3	1.251E+03	7.638E+02	4.274E+02	1.685E+02	5.060E+01	1.201E+01	3.289E+00	1.893E+00
13.4	1.363E+03	8.272E+02	4.606E+02	1.801E+02	5.342E+01	1.247E+01	3.353E+00	1.913E+00
13.5	1.485E+03	8.960E+02	4.964E+02	1.925E+02	5.641E+01	1.294E+01	3.418E+00	1.934E+00
13.6	1.618E+03	9.707E+02	5.351E+02	2.057E+02	5.958E+01	1.344E+01	3.485E+00	1.955E+00
13.7	1.763E+03	1.052E+03	5.770E+02	2.200E+02	6.294E+01	1.396E+01	3.554E+00	1.976E+00
13.8	1.921E+03	1.140E+03	6.221E+02	2.353E+02	6.650E+01	1.450E+01	3.625E+00	1.998E+00
13.9	2.094E+03	1.235E+03	6.709E+02	2.516E+02	7.028E+01	1.506E+01	3.697E+00	2.020E+00
14.0	2.282E+03	1.339E+03	7.237E+02	2.692E+02	7.429E+01	1.565E+01	3.772E+00	2.042E+00
14.1	2.487E+03	1.451E+03	7.807E+02	2.881E+02	7.854E+01	1.627E+01	3.848E+00	2.065E+00
14.2	2.712E+03	1.574E+03	8.423E+02	3.083E+02	8.305E+01	1.691E+01	3.927E+00	2.089E+00
14.3	2.957E+03	1.706E+03	9.089E+02	3.300E+02	8.784E+01	1.758E+01	4.007E+00	2.112E+00
14.4	3.224E+03	1.850E+03	9.810E+02	3.532E+02	9.292E+01	1.828E+01	4.090E+00	2.137E+00
14.5	3.516E+03	2.007E+03	1.059E+03	3.782E+02	9.832E+01	1.901E+01	4.175E+00	2.161E+00
14.6	3.834E+03	2.177E+03	1.143E+03	4.050E+02	1.040E+02	1.978E+01	4.262E+00	2.186E+00
14.7	4.182E+03	2.362E+03	1.234E+03	4.338E+02	1.101E+02	2.058E+01	4.352E+00	2.212E+00
14.8	4.561E+03	2.562E+03	1.333E+03	4.647E+02	1.166E+02	2.142E+01	4.444E+00	2.238E+00
14.9	4.976E+03	2.780E+03	1.439E+03	4.979E+02	1.234E+02	2.229E+01	4.539E+00	2.264E+00
15.0	5.428E+03	3.017E+03	1.555E+03	5.336E+02	1.307E+02	2.321E+01	4.636E+00	2.291E+00
15.1	5.923E+03	3.274E+03	1.679E+03	5.719E+02	1.385E+02	2.416E+01	4.736E+00	2.319E+00
15.2	6.462E+03	3.554E+03	1.814E+03	6.130E+02	1.467E+02	2.516E+01	4.839E+00	2.347E+00
15.3	7.052E+03	3.858E+03	1.961E+03	6.572E+02	1.554E+02	2.621E+01	4.944E+00	2.376E+00
15.4	7.696E+03	4.189E+03	2.119E+03	7.047E+02	1.647E+02	2.730E+01	5.053E+00	2.405E+00
15.5	8.399E+03	4.548E+03	2.290E+03	7.557E+02	1.746E+02	2.845E+01	5.164E+00	2.434E+00
15.6	9.168E+03	4.939E+03	2.475E+03	8.106E+02	1.851E+02	2.965E+01	5.279E+00	2.464E+00
15.7	1.001E+04	5.364E+03	2.676E+03	8.696E+02	1.963E+02	3.090E+01	5.396E+00	2.495E+00
15.8	1.092E+04	5.826E+03	2.893E+03	9.330E+02	2.082E+02	3.221E+01	5.517E+00	2.526E+00
15.9	1.193E+04	6.328E+03	3.129E+03	1.001E+03	2.208E+02	3.359E+01	5.642E+00	2.558E+00
16.0	1.302E+04	6.874E+03	3.384E+03	1.074E+03	2.343E+02	3.503E+01	5.770E+00	2.591E+00
16.1	1.422E+04	7.468E+03	3.660E+03	1.153E+03	2.486E+02	3.653E+01	5.901E+00	2.624E+00
16.2	1.553E+04	8.115E+03	3.959E+03	1.238E+03	2.638E+02	3.811E+01	6.036E+00	2.658E+00
16.3	1.695E+04	8.818E+03	4.283E+03	1.329E+03	2.800E+02	3.976E+01	6.176E+00	2.692E+00
16.4	1.852E+04	9.583E+03	4.634E+03	1.427E+03	2.972E+02	4.150E+01	6.319E+00	2.727E+00
16.5	2.022E+04	1.042E+04	5.014E+03	1.533E+03	3.156E+02	4.331E+01	6.466E+00	2.763E+00
16.6	2.209E+04	1.132E+04	5.427E+03	1.647E+03	3.351E+02	4.521E+01	6.617E+00	2.799E+00
16.7	2.413E+04	1.231E+04	5.873E+03	1.769E+03	3.559E+02	4.720E+01	6.773E+00	2.836E+00
16.8	2.636E+04	1.338E+04	6.357E+03	1.900E+03	3.781E+02	4.929E+01	6.933E+00	2.874E+00
16.9	2.880E+04	1.455E+04	6.882E+03	2.042E+03	4.017E+02	5.147E+01	7.098E+00	2.913E+00
17.0	3.147E+04	1.582E+04	7.451E+03	2.195E+03	4.268E+02	5.377E+01	7.267E+00	2.952E+00
17.1	3.438E+04	1.720E+04	8.068E+03	2.359E+03	4.536E+02	5.617E+01	7.442E+00	2.992E+00
17.2	3.757E+04	1.871E+04	8.737E+03	2.536E+03	4.821E+02	5.869E+01	7.621E+00	3.033E+00
17.3	4.105E+04	2.034E+04	9.462E+03	2.726E+03	5.125E+02	6.134E+01	7.806E+00	3.074E+00
17.4	4.487E+04	2.213E+04	1.025E+04	2.931E+03	5.449E+02	6.411E+01	7.996E+00	3.116E+00
17.5	4.904E+04	2.407E+04	1.110E+04	3.152E+03	5.795E+02	6.702E+01	8.192E+00	3.160E+00
17.6	5.360E+04	2.619E+04	1.203E+04	3.390E+03	6.163E+02	7.007E+01	8.393E+00	3.204E+00
17.7	5.858E+04	2.849E+04	1.303E+04	3.647E+03	6.556E+02	7.327E+01	8.601E+00	3.248E+00
17.8	6.404E+04	3.100E+04	1.412E+04	3.923E+03	6.975E+02	7.663E+01	8.814E+00	3.294E+00
17.9	7.001E+04	3.374E+04	1.530E+04	4.221E+03	7.421E+02	8.015E+01	9.034E+00	3.341E+00
18.0	7.654E+04	3.671E+04	1.658E+04	4.541E+03	7.897E+02	8.385E+01	9.261E+00	3.388E+00
18.1	8.368E+04	3.996E+04	1.797E+04	4.887E+03	8.405E+02	8.774E+01	9.494E+00	3.437E+00
18.2	9.149E+04	4.349E+04	1.948E+04	5.260E+03	8.947E+02	9.182E+01	9.734E+00	3.486E+00
18.3	1.000E+05	4.734E+04	2.112E+04	5.662E+03	9.525E+02	9.610E+01	9.981E+00	3.537E+00
18.4	1.094E+05	5.153E+04	2.290E+04	6.095E+03	1.014E+03	1.006E+02	1.024E+01	3.588E+00
18.5	1.196E+05	5.610E+04	2.483E+04	6.563E+03	1.080E+03	1.053E+02	1.050E+01	3.640E+00
18.6	1.308E+05	6.108E+04	2.692E+04	7.066E+03	1.150E+03	1.103E+02	1.077E+01	3.694E+00
18.7	1.431E+05	6.651E+04	2.920E+04	7.610E+03	1.225E+03	1.155E+02	1.105E+01	3.748E+00
18.8	1.565E+05	7.242E+04	3.167E+04	8.196E+03	1.305E+03	1.210E+02	1.133E+01	3.804E+00
18.9	1.712E+05	7.887E+04	3.435E+04	8.828E+03	1.391E+03	1.267E+02	1.163E+01	3.860E+00
19.0	1.873E+05	8.589E+04	3.726E+04	9.510E+03	1.482E+03	1.328E+02	1.194E+01	3.918E+00
19.1	2.048E+05	9.355E+04	4.042E+04	1.025E+04	1.580E+03	1.391E+02	1.225E+01	3.977E+00
19.2	2.241E+05	1.019E+05	4.385E+04	1.104E+04	1.684E+03	1.458E+02	1.257E+01	4.037E+00
19.3	2.452E+05	1.110E+05	4.758E+04	1.190E+04	1.795E+03	1.528E+02	1.291E+01	4.099E+00
19.4	2.682E+05	1.209E+05	5.163E+04	1.282E+04	1.914E+03	1.602E+02	1.325E+01	4.161E+00

Table 1
(Continued)

T_{ex}/T_U	$\kappa = 2$	$\kappa = 3$	$\kappa = 4$	$\kappa = 6$	$\kappa = 10$	$\kappa = 20$	$\kappa = 50$	$\kappa = 100$
19.5	2.935E+05	1.317E+05	5.603E+04	1.382E+04	2.041E+03	1.679E+02	1.361E+01	4.225E+00
19.6	3.211E+05	1.435E+05	6.081E+04	1.490E+04	2.176E+03	1.761E+02	1.397E+01	4.290E+00
19.7	3.514E+05	1.564E+05	6.600E+04	1.606E+04	2.321E+03	1.847E+02	1.435E+01	4.356E+00
19.8	3.845E+05	1.704E+05	7.164E+04	1.731E+04	2.476E+03	1.937E+02	1.474E+01	4.424E+00
19.9	4.208E+05	1.857E+05	7.777E+04	1.867E+04	2.642E+03	2.032E+02	1.514E+01	4.493E+00
20.0	4.606E+05	2.024E+05	8.444E+04	2.013E+04	2.819E+03	2.132E+02	1.555E+01	4.564E+00

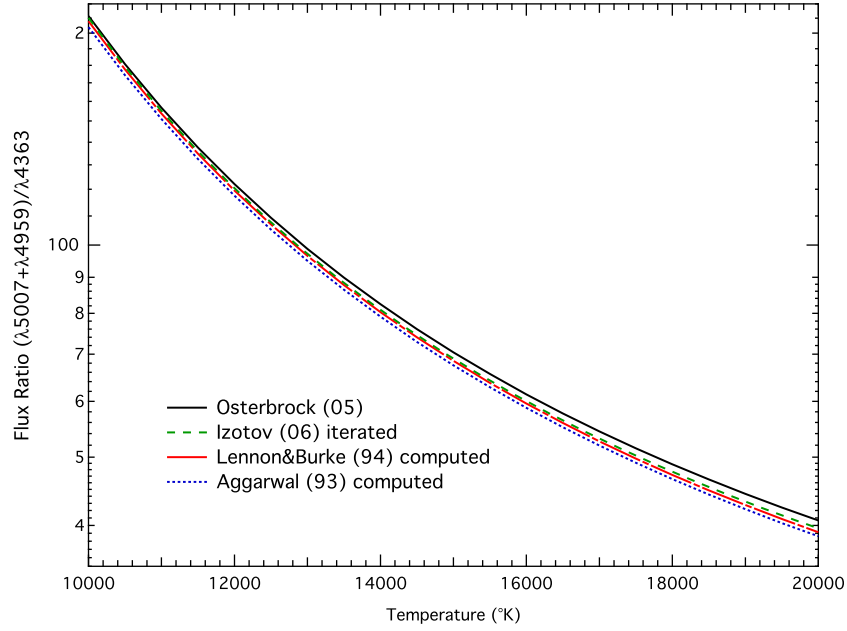


Figure 7. [O III] line flux ratio vs. temperature for M-B-distributed electrons computed from different methods and by different authors.

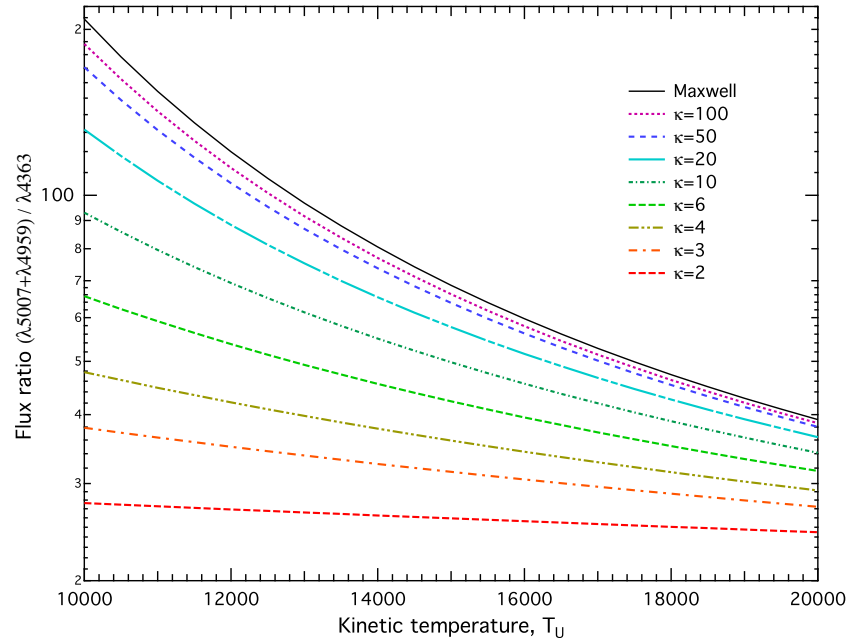


Figure 8. [O III] line flux ratio vs. kinetic temperature for the range $\kappa = 2 \rightarrow 100$, compared to the computed Lennon & Burke (1994) equilibrium data, labeled Maxwell in the figure. (extended data in Table 2.)

a significant effect on electron temperatures measured using the [O III] lines. The same result is true for other collisionally excited lines, [O II], [S II], and [N II], but to differing extents, owing to the different collisional excitation energy thresholds

for the upper and lower states. The differences in apparent electron temperatures calculated using different collisionally excited species allow us to obtain an estimate of the effective value of κ for remote H II regions, as we show in Section 6.

Table 2
[O III] Line Flux Ratios versus Kinetic Temperature T_U (See Figure 8)

T_U (K)	$\kappa = 2$	$\kappa = 3$	$\kappa = 4$	$\kappa = 6$	$\kappa = 10$	$\kappa = 20$	$\kappa = 50$	$\kappa = 100$	Maxwell
5000	29.7012	48.1983	72.5995	138.179	322.942	914.582	2365.64	3551.70	5678.96
5500	29.4789	46.8930	69.0278	125.368	270.262	674.143	1513.02	2121.70	3117.32
6000	29.2609	45.6613	65.7814	114.480	229.899	515.460	1032.33	1372.76	1891.11
6500	29.0469	44.4974	62.8208	105.148	198.350	406.285	741.598	945.508	1238.84
7000	28.8369	43.3962	60.1122	97.0852	173.257	328.495	555.442	684.565	861.973
7500	28.6308	42.3530	57.6269	90.0701	152.988	271.388	430.514	516.106	629.358
8000	28.4285	41.3637	55.3402	83.9261	136.389	228.376	343.322	402.263	477.847
8500	28.2299	40.4242	53.2305	78.5127	122.629	195.251	280.418	322.330	374.680
9000	28.0348	39.5313	51.2794	73.7162	111.094	169.241	233.734	264.362	301.772
9500	27.8433	38.6815	49.4707	69.4446	101.329	148.467	198.235	221.147	248.601
10000	27.6551	37.8721	47.7904	65.6223	92.9877	131.622	170.664	188.154	208.767
10500	27.4702	37.1003	46.2259	62.1868	85.8035	117.779	148.851	162.440	178.225
11000	27.2886	36.3637	44.7665	59.0863	79.5699	106.266	131.311	142.033	154.330
11500	27.1102	35.6602	43.4024	56.2774	74.1239	96.5858	117.002	125.577	135.302
12000	26.9348	34.9875	42.1252	53.7234	69.3362	88.3683	105.179	112.119	119.912
12500	26.7623	34.3438	40.9273	51.3936	65.1029	81.3305	95.2955	100.973	107.292
13000	26.5928	33.7274	39.8019	49.2613	61.3397	75.2547	86.9487	91.6369	96.8137
13500	26.4262	33.1366	38.7429	47.3043	57.9780	69.9709	79.8335	83.7378	88.0182
14000	26.2623	32.5699	37.7450	45.5029	54.9612	65.3451	73.7166	76.9927	80.5612
14500	26.1012	32.0260	36.8034	43.8406	52.2424	61.2705	68.4173	71.1849	74.1819
15000	25.9426	31.5035	35.9135	42.3027	49.7824	57.6609	63.7940	66.1462	68.6799
15500	25.7867	31.0013	35.0715	40.8766	47.5483	54.4468	59.7342	61.7444	63.8991
16000	25.6333	30.5183	34.2739	39.5513	45.5125	51.5708	56.1483	57.8745	59.7166
16500	25.4823	30.0534	33.5173	38.3170	43.6512	48.9858	52.9635	54.4524	56.0347
17000	25.3338	29.6057	32.7988	37.1652	41.9444	46.6528	50.1207	51.4099	52.7748
17500	25.1876	29.1742	32.1158	36.0884	40.3747	44.5389	47.5714	48.6915	49.8733
18000	25.0437	28.7582	31.4658	35.0798	38.9272	42.6167	45.2751	46.2514	47.2781
18500	24.9020	28.3569	30.8466	34.1336	37.5891	40.8628	43.1986	44.0517	44.9463
19000	24.7625	27.9695	30.2562	33.2444	36.3492	39.2574	41.3137	42.0609	42.8424
19500	24.6252	27.5953	29.6926	32.4074	35.1975	37.7835	39.5966	40.2524	40.9365
20000	24.4900	27.2337	29.1543	31.6185	34.1256	36.4266	38.0273	38.6038	39.2038

Note. Maxwell figures computed using Lennon & Burke (1994) Ω data.

5. THE ABUNDANCE DISCREPANCY PROBLEM

Discrepancies between measurements made using various temperature-sensitive ion line ratios have been observed in both H II regions and PNe. Recombination temperatures (derived from the Balmer and Paschen jumps) are systematically lower than temperatures derived from collisionally excited line ratios. Systematic differences in temperature are also observed between collisionally excited line ratios of different ionic species (García-Rojas & Esteban 2007; Izotov et al. 2006). This results in systematically different chemical abundances derived by optical recombination lines (ORLs) and collisionally excited lines (CELs), a problem dating back to Wyse (1942) and first discussed in detail by Torres-Peimbert & Peimbert (1977). There are also systematic differences between abundances determined using either direct measurements of ionic temperatures, correcting observed ionic abundances for unseen ionization stages (the T_e method), or using the intensities of strong emission lines relative to the Hydrogen recombination lines (the strong line method). Collectively, these are known as the abundance discrepancy problem (García-Rojas et al. 2006; García-Rojas & Esteban 2007).

The confusion surrounding this issue has been well summarized by Stasińska (2004):

“It has been known for several decades that optical recombination lines [ORL] in PNe and H II regions indicate higher abundances than collisionally excited lines [CEL].

The ORL abundances are higher than CEL abundances by factors of about 2 for most PNe, discrepancies over a factor 5 are found in about 5% of the PNe and can reach factors as large as 20. For a given nebula, the discrepancies for the individual elements C, N, O, Ne are found to be approximately of the same magnitude.

The explanations most often invoked are: i) temperature fluctuations, ii) incorrect atomic data, iii) fluorescent excitation, iv) upward bias in the measurement of weak line intensities, v) blending with other lines, vi) abundance inhomogeneities. None of them is completely satisfactory, some are now definitely abandoned.”

The possibility that the abundance discrepancy problem could be generated by the techniques used to measure abundances was recently investigated by López-Sánchez et al. (2012), using a grid of theoretical models to eliminate any systematics of observational errors. Although systematic errors were found in a number of empirical strong line techniques, the classical electron temperature + ionization correction factor technique works surprisingly well. Clearly, the technique itself is not at fault.

Perhaps the most successful attempt to account for the abundance discrepancy problem has been to postulate the existence of small-scale temperature fluctuations as first proposed by Peimbert & Costero (1969), known as the “ t^2 ” method, and applied widely since; see e.g., Peimbert (2003) and references

therein. To some extent, electron temperature fluctuations (if real) act in a similar way to a κ -distributed electron population, in that both weight CELs toward higher temperature. However, we are missing an obvious physical explanation of why microfluctuations in temperature should exist and persist in the first place.

The κ approach has major advantages over the t^2 method: it is simple; it is consistent over many objects and atomic species; it arises directly from Tsallis q -nonextensive statistics; the physics of ionized plasmas in H II regions and PNe provides several mechanisms capable of generating the suprathermal distribution tails; it has been shown to describe accurately numerous directly measured electron energy distributions in the solar system; and it explains behavior over an energy range of at least three orders of magnitude, from low-energy recombination line electrons to the high ionization energies in the solar corona. The relationship between the t^2 approach and the κ -distribution is explored further in Appendix B.

6. THE DETERMINATION OF κ

6.1. H II Regions

As noted earlier (Equation (8)), a κ -distribution with kinetic temperature T_U can be characterized at low electron energies below the peak of the distribution by a “core” Boltzmann distribution with an effective temperature $T_{\text{core}} = (\kappa - 3/2)T_U/\kappa$. Since T_{core} is systematically lower than T_U , and as it is the energy distribution of these low-energy electrons that determines the recombination temperature ($T_{\text{rec}} \equiv T_{\text{core}}$), it is clear that in a κ -distribution the recombination rate is systematically enhanced. These same low-energy electrons also determine the size of the Balmer and Paschen discontinuities of Hydrogen, so that the measured Balmer and Paschen break temperatures will reflect T_B , rather than T_U .

At the same time, lines with excitation temperatures comparable to T_U may be either mildly enhanced or suppressed in a κ -distribution, but lines with excitation temperatures well above T_U are strongly enhanced by the power-law tail of high-energy electrons present in the κ -distribution. This has the effect of enhancing the apparent electron temperature inferred using well-known temperature-sensitive line ratios such as [O III] 4363 Å/5007,4959 Å, [S II] 4069,76 Å/6717,31 Å, [N II] 5755 Å/6548,84 Å, or [O II] 7318,24 Å/3726,29 Å. The degree of enhancement of the inferred temperature, compared to T_U , is strongly dependent on T_{ex} , the excitation temperature of the upper levels involved in these transitions. Those ions in which T_{ex} is much greater than T_U will have their inferred collisional excitation temperature, T_{CEL} , very strongly enhanced over T_U , while those for which T_{ex} is comparable to T_U will show little change ($T_{\text{CEL}} \sim T_U$).

These properties of the κ -distribution can be used as the basis for the determination of κ from spectrophotometric observations of both H II regions and PNe.

We can test the κ -distribution hypothesis using the excellent echelle spectrophotometry which has been gathered by a number of authors in recent years. For Galactic H II regions, we have data in M 42 (Esteban et al. 2004), NGC 3576, S311 (García-Rojas et al. 2004), M20 & NGC 3603 (García-Rojas et al. 2006), and M 8 & M 17 (García-Rojas & Esteban 2007). For the extragalactic H II regions, we have data for 30 Dor (Peimbert 2003), NGC 5253 (López-Sánchez et al. 2007), NGC 595, NGC 604, VS 24, VS 44, NGC 2365, and K 932 (Esteban et al. 2009).

One of the strongest tests of the validity of the κ -distribution is the comparison of the [O II] 7318,24 Å/3726,29 Å and [S II] 4069,76 Å/6717,31 Å temperatures. These ions have very similar ionization potentials and are therefore distributed in a very similar way in the nebula. The photoionization models used by López-Sánchez et al. (2012) have line emission weighted temperatures in the O II and S II zones which differ from each other by less than 400 K over the abundance range 0.3–3.0 times solar. However, the excitation temperatures of the lines are quite different. For the [S II] 4069,76 Å lines, $T_{\text{ex}} = 35,320$ K, and for the [S II] 6717,31 Å lines, $T_{\text{ex}} = 21,390$ K. In the case of [O II] 7318,24 Å, $T_{\text{ex}} = 58,220$ K, while for the 3726,29 Å lines, $T_{\text{ex}} = 38,590$ K. Thus, the [O II] lines are much more sensitive to the high-energy tail of the κ -distribution than are the [S II] lines. On this basis, one would expect higher temperatures to be derived from the [O II] line ratio than from the [S II] line ratios in the presence of a κ -distribution.

We have computed for the observed data the effect that a κ -distribution has on the inferred collisional excitation temperature, T_{CEL} , of these ions. This is shown in Figure 9(a). The observations suggest that the [O II] temperatures are indeed higher than the [S II] temperatures, and that this difference can be accounted for in most of the H II regions by $20 \gtrsim \kappa \gtrsim 10$.

As an alternative approach, we show in Figure 9(b) the average of the inferred collisional excitation temperatures for the [O II] and [N II] ions compared with that of the [S II] ion. For the [O II] and [N II] ions, the sensitivity to κ is not as great as for the [O II] lines alone, but the errors in the temperature determination produced by assumptions about the dust extinction curve are reduced. Again, the [S II] temperatures are lower. The inferred range of κ is somewhat wider, but most H II regions are still consistent with $20 \gtrsim \kappa \gtrsim 10$.

Because the recombination temperature, T_B , is appreciably lower than the kinetic temperature T_U , which is itself lower than the excitation temperature for collisionally excited line ratios, T_{ex} , a comparison of recombination temperatures and inferred line temperatures is strongly sensitive to the choice of κ . The recombination temperatures, T_{REC} , should be significantly lower than the collisionally excited line temperatures, T_{CEL} , in the presence of a κ -distribution. Again, this is clearly shown in the analysis of the observed H II region spectra.

In Figures 9(c) and (d), we show this comparison for the H II regions, using the excitation temperature given by the average of the [O II] and [N II] line ratios and by the [O III] line ratio, respectively. How well these determine κ depends on which of the ionic species is the dominant ionization stage in the nebula. For cooler exciting stars, [O II] and [N II] line ratios are the better ones to use, but when the central star(s) is hot enough to ionize helium to He II in the bulk of the nebula, then the [O III] line ratio is the better one to use. From Figures 9(c) and (d), it would appear that $\kappa \sim 20$, or even higher. Because the upper state of [O III] has the highest excitation temperature, it is the most sensitive of all the ions to the high-energy electrons, and therefore lower values of κ have greater effects.

6.2. Planetary Nebulae

High-quality spectrophotometry also exists for many PNe, although published values of electron temperatures for many ions is rather sparse. However, rather complete data exist for temperatures determined from the Balmer discontinuity and from the [O III] line ratio. The direct comparison of these should

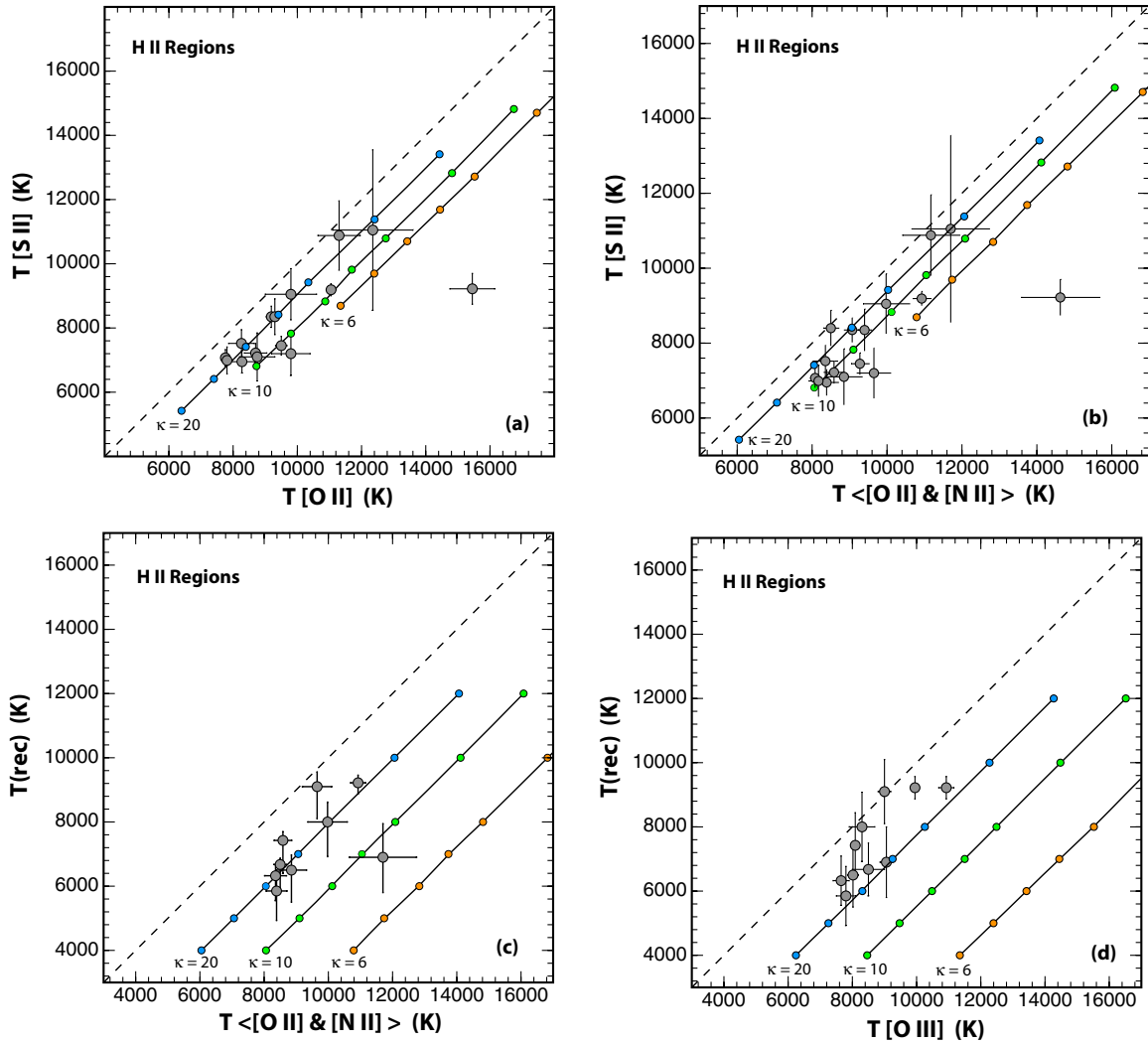


Figure 9. Measured temperatures in H II regions compared with what would be expected if the electrons have a κ -distribution. Panel (a) compares the inferred excitation temperatures of the [O II] and [S II] ions, panel (b) the average of the [O II] and [N II] ions with the [S II] ion. Panels (c) and (d) compare the recombination temperatures given by the mean of the Balmer and the Paschen break temperatures with the mean excitation temperature given by the average of the [O II] and [N II] line ratios, panel (c), and that of the [O III] line ratio, panel (d). Most H II regions appear to have $20 \gtrsim \kappa \gtrsim 10$.

(A color version of this figure is available in the online journal.)

be a fairly reliable means of estimating κ , since the O III ion is most often the dominant ionization stage in PNe.

We have taken data from Tsamis et al. (2003), Liu et al. (2004), Zhang et al. (2004), Wesson et al. (2005), Wang & Liu (2007), and Fang & Liu (2011). These data are plotted in Figure 10, along with the expectation for $\kappa = 6, 10$, and 20 . The points with error bars are from Zhang et al. (2004). Again, the results are consistent with $\kappa > 10$ in most cases, i.e., a mild departure from an equilibrium electron energy distribution. A few points lie above the line of equality of temperatures shown by the dotted line, corresponding to $\kappa = \infty$. However, many of these are consistent with no departure from an M-B distribution, within the observational errors. Of course, it is likely that local temperature and density fluctuations in the PNe contribute to the measured results, and it is not obvious what the contributions are from the various effects.

There are two apparent trends in Figure 10: both cooler objects and objects with high [O III] electron temperatures tend to show greater deviations from equilibrium (smaller inferred κ). For high electron temperature objects, the energetic stellar winds from the hot central star are likely to lead to

significant suprathermal heating of the ionized plasma, leading to lower values of κ . Indeed, some of the points identified by name (NGC 2440 and NGC 6302) are famous Peimbert Type I PNe, known to contain the most luminous and massive central stars. Among the rest, IC 4997 is a young PNe which also contains a Wolf-Rayet type central star, subject to rapid mass-loss.

The coolest objects tend to be more metal rich, and/or of lower excitation class. As a result, the excitation is dominated by the high-energy tail of the energy distribution, as illustrated in Figure 5: κ effects for [O III] become more apparent. These and other characteristics of the κ -distribution will be the subject of detailed modeling in future papers.

The results for both PNe and H II regions are consistent with mild departures from equilibrium ($\kappa \gtrsim 10$). It is interesting to note that in the analysis of the observed spectra, extreme values of κ are not required. The implied departures from an M-B distribution are quite small, but their effect on the nebular diagnostics is quite gross, with serious implications for the chemical abundance determinations in both classes of object. Large departures from the M-B distribution in either PNe or H II

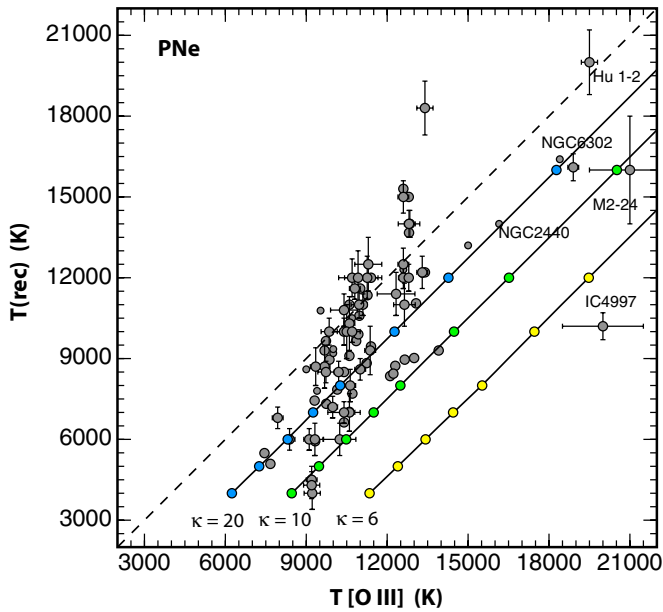


Figure 10. As Figure 9(d), but for planetary nebulae.

(A color version of this figure is available in the online journal.)

regions (lower values of κ) would in any case not be expected, since at the peak of the energy distribution the mean collision time between electrons is short.

7. CONCLUSION

In this paper, we have explored the implications for temperature and metallicity measurement in H II regions and PNe of assuming a non-equilibrium κ electron energy distribution. We have shown that κ -distributions provide apparent electron temperatures measured from forbidden line ratios which are systematically higher than the kinetic temperature T_U . Assuming κ -distributed electron energies appears to resolve the long standing discrepancies in temperatures measured using the collisional excitation lines of different atomic species, and those calculated using the bound-free recombination continuum. Using high-quality published spectra, we have shown that for objects where the spectra of more than one appropriate atomic species is identifiable, it is possible to estimate a value for the effective value of κ . $\kappa \sim 20$ is a good fit to many of the measurements. This value does not require a substantial redistribution of the population to be achieved, meaning that any of several means of generating high-energy electrons should be capable of sustaining the non-equilibrium distribution.

The κ -distribution offers an important new insight into the physics of gaseous nebulae, both in the Galaxy and elsewhere. It is implausible that thermal equilibrium applies throughout in H II regions and PNe, and the fact that the κ -distribution is able to explain long standing discrepancies is a strong indication that non-equilibrium is a valid assumption. It should enable more accurate estimates of temperature and metallicity in these regions. A detailed investigation into the implications for metallicity measurements will be provided in a future paper.

The authors thank the anonymous referee for helpful suggestions on the document structure. M. Dopita acknowledges

the support of the Australian Research Council (ARC) through Discovery project DP0984657.

Note added in proof. Our attention has been drawn to simulations of the magnetohydrodynamics of H II regions by Henney et al. (2009) and Arthur et al. (2011), in which they show that, in their models, β , the ratio of thermal to magnetic energy, is usually greater than unity, and that the observed filamentary structures (Figure 11) arise naturally in the simulations. The fact that these features appear to be magnetohydrodynamic in origin is evidence for the widespread presence of magnetic fields in H II regions.

APPENDIX A

EVIDENCE FOR MAGNETIC FIELDS IN MILKY WAY H II REGIONS

In order for magnetic energy to be an important source of non-thermal electrons, we require β , the ratio of the thermal to magnetic energy, to be less than unity. Direct measurements of β have been made for H II regions using Faraday rotation observations (Harvey-Smith et al. 2011; Rodríguez et al. 2012). These reveal values of $\beta \sim 5$. However, these measurements do not reveal the full strength of the magnetic field if there is turbulence, they indicate only the size of the organized field. They should therefore be taken as imposing a lower bound on the true magnetic field. However, recent evidence on the warm ionized medium (Gaensler et al. 2011) suggests that magnetic turbulence dominates at small scales. Finally, it is generally believed that the magnetic turbulence in the HI phase leads to equipartition ($\beta \sim 1$). Let us take this as a working hypothesis and ask what happens across an ionization front in an H II region.

Let the HI region be characterized by a density ρ_0 , temperature T_0 , pressure P_0 , magnetic field \vec{B}_0 , and sound speed $c_0 = (\gamma P_0 / \rho_0)^{1/2}$. The Alfvén velocity in the gas is $v_A^2 = B_0^2 / 4\pi\rho$. In the HI region ahead of the ionization front, if we assume that the gas is turbulently supported, then $\beta_0 \sim 1$, i.e., $(2/\gamma)(c_0/v_A)^2 \sim 1$, on average. We can resolve the magnetic field into components parallel to the gas flow, $B_0^{\parallel} \sim B_0/\sqrt{3}$, and perpendicular to the gas flow (in the plane of the ionization front), $B_0^{\perp} \sim B_0\sqrt{2/3}$. These components will fluctuate on the scale of the pressure-supported turbulent cells in the HI region, so they relate to the mean field only in a stochastic fashion.

Now consider what happens on the other side of the ionization front, where the sound speed is c_1 , the outflow Mach number is \mathcal{M} , and the hydrodynamic variables are ρ_1 , P_1 , T_1 , B_1^{\parallel} and B_1^{\perp} . The ratio of the densities is obtained by equating the pre-ionization pressure to the post-ionization pressure, accounting for the recoil momentum of the ionized plasma:

$$\frac{\rho_0 c_0^2}{\gamma} = \frac{\rho_1 c_1^2}{\gamma} + \mathcal{M}^2 \rho_1 c_1^2. \quad (\text{A1})$$

The component of the magnetic field perpendicular to the flow direction is stretched (reduced) in the post-ionization zone by the ratio ρ_1/ρ_0 , and the local gas pressure is decreased in the ratio $1/(1 + \gamma\mathcal{M}^2)$. Therefore,

$$\beta_1^{\perp} \sim \frac{3}{2} \left(\frac{1}{1 + \gamma\mathcal{M}^2} \right) \left(\frac{\rho_0}{\rho_1} \right)^2. \quad (\text{A2})$$

Thus, all magnetic pressure support is effectively lost in this plane. However, parallel to the flow, the post-shock magnetic

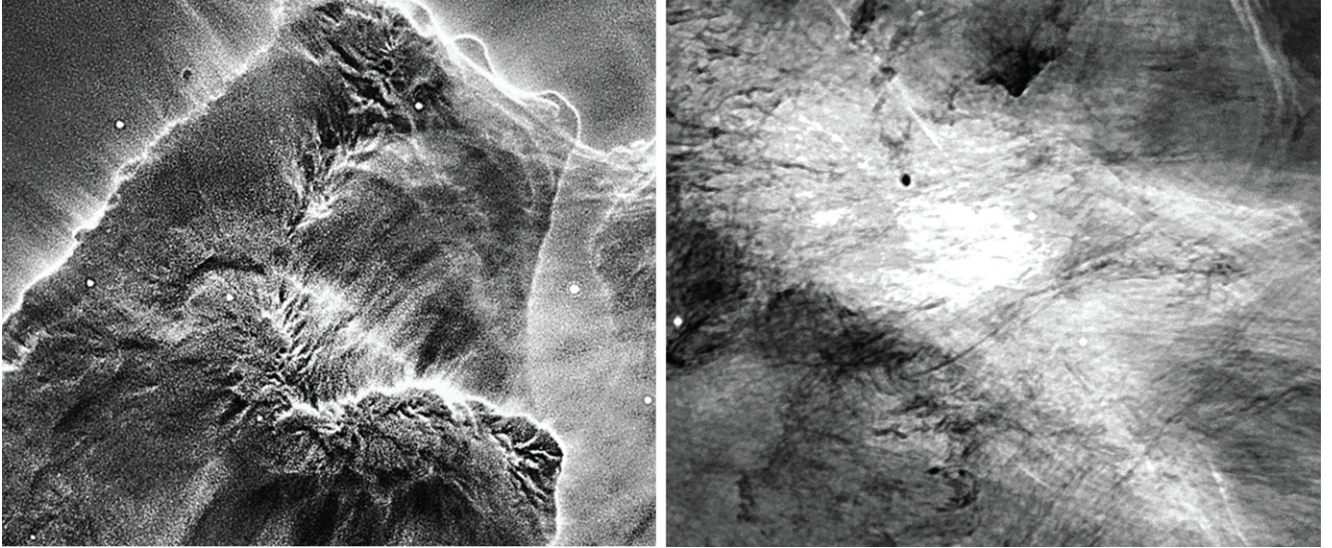


Figure 11. Portions of *HST* images of the η Carina nebula (left) and M17 (right) taken with the ACS. These images have been processed by an unsharp mask to bring up the microstructure. Both images display magnetically dominated microstructures aligned with the outflow direction. The scales of these microfilaments is of order of the size of the solar system.

field is unchanged by the ionization, and therefore

$$\beta_1^{\parallel} \sim 3 \left(\frac{1}{1 + \gamma \mathcal{M}^2} \right) < 1. \quad (\text{A3})$$

Thus, the magnetic pressure dominates the thermal pressure in this direction. The turbulent origin of the magnetic field in the molecular cloud ensures that β_1^{\parallel} is rapidly fluctuating both in magnitude and direction, which will naturally assist magnetic reconnection and inertial Alfvén wave formation.

This magnetic field, highly aligned to the flow direction and showing strong fluctuations on the small scale provides a natural explanation for the filamentary structure of the ionized plasma seen very clearly in the η Carina and M17 H II regions observed by the Advanced Camera for Surveys (ACS) on the *Hubble Space Telescope* (*HST*; see Figure 11, below).

In the case of η Carina, the ionized filaments are seen as bright “hairs” originating at the ionization front. These bright regions correspond to the regions of low magnetic field, given that the gas flow from the ionization front has to be force free in the plane of the ionization front. In the case of M17, we are seeing non-ionized regions of low magnetic field and high dust optical depth “combed out” by the expanding ionized plasma. These filaments are only a few AU in diameter, and have an aspect ratio of up to 50 : 1. The implied atomic densities are of the order of 10^5 atoms cm^{-3} .

APPENDIX B

THE κ -DISTRIBUTION AND THE TEMPERATURE FLUCTUATION (t^2) METHOD

As early as 1967, Peimbert proposed that abundance discrepancies might be explained by spatial temperature variations within an H II region (Peimbert 1967). The approach is characterized by a parameter, t^2 , the mean square fractional temperature fluctuation (assumed to have a Gaussian distribution in space). While it is certain that there are spatial variations in temperature, those caused naturally by the radial temperature variation in the H II region are usually insufficient to explain observations, and the cause of the larger values of t^2 implied by the observations remains unknown. However, the t^2 approach

has been widely used, with mixed success (e.g., Peña-Guerrero et al. 2012; García-Rojas & Esteban 2007; Esteban 2002; Kingdon & Ferland 1995). Detailed discussions of the technique are given in Stasińska (2004) and Kingdon & Ferland (1995).

The t^2 parameter is estimated by solving equations involving the collisionally excited line temperature(s) and the recombination line temperature (Kingdon & Ferland 1995). But as Kingdon & Ferland (1995) also argued, “while temperature fluctuations may result in non-negligible abundance corrections in some objects, they are insufficient to resolve the abundance discrepancy.”

There is, however, a connection between the t^2 method for resolving abundance discrepancies and the κ -distribution. Livadiotis et al. (2011) noted that “ κ -distributions can be derived from the superposition of Maxwellian distributions by considering a non-fixed temperature that is characterized by a certain (continuous or discrete) density distribution of temperatures.” Thus,

$$f_{\kappa}(E, T_U, \kappa) = \sum_{i=0}^{\infty} \Phi(f_{\text{Max}}(E, T_i), \kappa), \quad (\text{B1})$$

where Φ can, in theory, be determined from the expressions in Equations (6) and (7). The necessity to include Maxwellian distributions in the series with extreme temperatures to provide the suprathermal tail at high energies is, of course, non-physical, and the series needs to be truncated. Nonetheless, expressed this way, the κ -distribution can be seen as a generalization of the t^2 method.

REFERENCES

- Aggarwal, K. M. 1994, *ApJS*, **85**, 197
 Aggarwal, K. M., & Keenan, F. P. 1999, *ApJS*, **123**, 311
 Aldrovandi, S. M. V., & Gruenwald, R. D. 1985, *A&A*, **147**, 331
 Arthur, S. J., Henney, W. J., Mellema, G., et al. 2011, *MNRAS*, **414**, 1747
 Dopita, M. A., & Sutherland, R. S. 2000, *ApJ*, **539**, 742
 Esteban, C. 2002, *RevMexAA Ser. Conf.*, **12**, 56
 Esteban, C., Bresolin, F., Peimbert, M., et al. 2009, *ApJ*, **700**, 654
 Esteban, C., Peimbert, M., García-Rojas, J., et al. 2004, *MNRAS*, **355**, 229
 Fang, X., & Liu, X.-W. 2011, *MNRAS*, **415**, 181

- Gaensler, B. M., Haverkorn, M., Burkhart, B., et al. 2011, *Nature*, **478**, 214
- García-Rojas, J., & Esteban, C. 2007, *ApJ*, **670**, 457
- García-Rojas, J., Esteban, C., Peimbert, A., et al. 2005, *MNRAS*, **362**, 301
- García-Rojas, J., Esteban, C., Peimbert, M., et al. 2004, *ApJS*, **153**, 501
- García-Rojas, J., Esteban, C., Peimbert, M., et al. 2006, *MNRAS*, **368**, 253
- Harvey-Smith, L., Madsen, G. J., & Gaensler, B. M. 2011, *ApJ*, **736**, 83
- Hebb, M. H., & Menzel, D. H. 1940, *ApJ*, **92**, 408
- Henney, W. J., Arthur, S. J., DeColle, F., & Mellema, G. 2009, *MNRAS*, **398**, 157
- Hummer, D. G., Berrington, K. A., Eissner, W., et al. 1993, *A&A*, **279**, 298
- Izotov, Y. I., Stasińska, G., Meynet, G., Guseva, N. G., & Thuan, T. X. 2006, *A&A*, **448**, 955
- Kingdon, J. B., & Ferland, G. J. 1995, *ApJ*, **450**, 691
- Lennon, D. J., & Burke, V. M. 1994, *A&AS*, **103**, 273
- Leubner, M. P. 2002, *Ap&SS*, **282**, 573
- Liu, Y., Liu, X.-W., Luo, S.-G., & Barlow, M. J. 2004, *MNRAS*, **353**, 1231
- Livadiotis, G., & McComas, D. J. 2010, *ApJ*, **714**, 971
- Livadiotis, G., & McComas, D. J. 2009, *J. Geophys. Res.*, **114**, A11105
- Livadiotis, G., & McComas, D. J. 2011, *ApJ*, **741**, 88
- Livadiotis, G., McComas, D. J., Dayeh, M. A., Funsten, H. O., & Schwadron, N. A. 2011, *ApJ*, **734**, 1
- López-Sánchez, A. R., Esteban, C., García-Rojas, J., Peimbert, M., & Rodríguez, M. 2007, *ApJ*, **656**, 168
- López-Sánchez, A. R., et al. 2012, *MNRAS* (in press)
- Osterbrock, D. E., & Ferland, G. J. 2005, *Astrophysics of Gaseous Nebulae and Active Galactic Nuclei* (2nd ed.; Sausalito, CA: University Science Books)
- Owoki, S. P., & Scudder, J. D. 1983, *ApJ*, **270**, 758
- Peimbert, A. 2003, *ApJ*, **584**, 735
- Peimbert, M. 1967, *ApJ*, **150**, 825
- Peimbert, M., & Costero, R. 1969, *Bol. Obs. Tonantzintla Tacubaya*, **5**, 3
- Peña-Guerrero, M. A., Peimbert, A., Peimbert, M., & Ruiz, M. T. 2012, *ApJ*, **746**, 115
- Petrini, D., & Da Silva, F. P. 1997, *A&A*, **317**, 262
- Pierrard, V., & Lazar, M. 2010, *Sol. Phys.*, **265**, 153
- Rodríguez, L. F., Gómez, Y., & Tafoya, D. 2012, *MNRAS*, **420**, 279
- Shizgal, B. D. 2007, *Ap&SS*, **312**, 227
- Shull, J. M., & Van Steenberg, M. E. 1985, *ApJ*, **298**, 268
- Spitzer, L., Jr. 1962, *Physics of Fully Ionized Gases* (2nd ed.; New York: John Wiley & Sons, Inc.)
- Stasińska, G. 2004, in *Cosmochemistry: The Melting Pot of the Elements*, ed. C. Esteban, R. J. García López, A. Herrero, & F. Sánchez (Cambridge: Cambridge Univ. Press), 115
- Torres-Peimbert, S., & Peimbert, M. 1977, *RevMexAA*, **2**, 181
- Treumann, R. A. 1999, *Phys. Scr.*, **59**, 19
- Treumann, R. A. 2001, *Ap&SS*, **277**, 81
- Tsallis, C., Levy, S. V. F., Souza, A. M. C., & Maynard, R. 1995, *Phys. Rev. Lett.*, **75**, 3589
- Tsamis, Y. G., Barlow, M. J., Liu, X.-W., Danziger, I. J., & Storey, P. J. 2003, *MNRAS*, **345**, 186
- Vasyliunas, V. M. 1968, *J. Geophys. Res.*, **73**, 2839
- Wang, W., & Liu, X.-W. 2007, *MNRAS*, **381**, 669
- Wesson, R., Liu, X.-W., & Barlow, M. J. 2005, *MNRAS*, **362**, 424
- Wyse, A. B. 1942, *ApJ*, **95**, 356
- Zhang, Y., Liu, X.-W., Wesson, R., et al. 2004, *MNRAS*, **351**, 935